frontiers | Frontiers in Earth Science

TYPE Original Research
PUBLISHED 17 January 2025
DOI 10.3389/feart.2024.1487605

Three-dimensional illumination analysis in pipe-like complexities by ray-tracing modeling

Zhihua Cui[1,2]*, Feng Tan[3,4] and Olusoji Lawrence Taiwo[2]

[1]College of Big Data and Software Engineering, Zhejiang Wanli University, Ningbo, China, [2]Department of Geology and Geophysics, University of Aberdeen, Aberdeen, United Kingdom, [3]Research and Development Center, BGP, CNPC, Zhuozhou, China, [4]State Key Laboratory of Oil and Gas Reservoir Geology and Exploitation, Chengdu University of Technology, Chengdu, China

Check for updates

OPEN ACCESS

EDITED BY
Alex Hay-Man Ng,
Guangdong University of Technology, China

REVIEWED BY
Maria Filomena Loreto,
National Research Council (CNR), Italy
Hui Sun,
Southwest Jiaotong University, China

*CORRESPONDENCE
Zhihua Cui,
geosciences.zhihuacui@gmail.com

RECEIVED 28 August 2024
ACCEPTED 16 December 2024
PUBLISHED 17 January 2025

CITATION
Cui Z, Tan F and Taiwo OL (2025) Three-dimensional illumination analysis in pipe-like complexities by ray-tracing modeling.
Front. Earth Sci. 12:1487605.
doi: 10.3389/feart.2024.1487605

Pipe-like formations are vertical, complex and shape-diverse subsurface structures. The accurate seismic interpretation is essential for understanding their fluid dynamics and environmental impacts. However, conventional seismic exploration techniques struggle to accurately resolve their critical areas due to a general decline in imaging quality. This challenge is significant due to their three-dimensional nature, as some exaggerated forms impact seismic imaging, despite appearing similar in 2D slices. This limited perspective is commonly used in the oil and gas industry. This study uses a forward solution based on ray-tracing modeling specifically designed for illumination studies to help understand the impact of boundary on illumination variation, complemented by robust geometric models and elastic information derived from reasonable interpretations. We explore the impact of boundary edge curvature on illumination. The findings indicate that low curvature edges allow more rays to penetrate deeper into the boundary areas, potentially achieving higher illumination. The potential distribution of low-illumination or shadow zones are then proposed on the horizontal attribute at the top of the root area, which may explain why internal structures are often poorly imaged. This suggests the possibility of internal ray preclusion, leading to local multiples that cannot be effectively received. This research supports and enhances the understanding of why conventional seismic methods have difficulty in fully addressing imaging quality for such complex structures. It provides a thoughtful basis for further geological interpretation of this and similar vertical structures under the constraints of seismic imaging technology.

KEYWORDS
pipe-like formation, ray-trace attribute, wavefront construction, illumination analysis, shadow zone

1 Introduction

Pipe-like complexities, e.g., fluid escape pipes, are substantial vertical formations that facilitate the movement of fluids and materials through vertically aligned fractures (Huuse and Mickelson, 2004; Petersen et al., 2010). These complex structures are widely detected around the world with high-resolution seismic technology, particularly along continental margins (Davies, 2003; Cartwright et al., 2007). They exhibit three-dimensional shapes with complex and diverse architectures, forming intricate networks of internal conduits that combine various sources of materials (Moss and Cartwright, 2010;

Cartwright and Santamarina, 2015). It is essential to investigate and deeply understand the internal details of these geological formations for advancing our knowledge of fluid dynamics, expulsion processes, and their geological and environmental implications, such as impacts on subsurface storage and greenhouse gas sequestration (Cartwright and Santamarina, 2015; Maestrelli et al., 2017).

The identification of these detailed structures heavily relies on seismic reflection data, as direct samples or outcrops are often unavailable. A more challenging issue is that, despite significant advances in seismic imaging technologies over the past decades, substantial challenges remain in accurately and fully resolving the critical parts of complex pipe-like structures (Løseth et al., 2011; Cartwright and Santamarina, 2015). This limitation highlights the need for enhanced imaging techniques to achieve more accurate geological interpretation.

One of the most critical issues is that imaging quality loss often occurs in these fluid pipe structures, especially with increasing depth (Moss and Cartwright, 2010; Cartwright and Santamarina, 2015). However, their discussions tend to focus on the imaging ambiguity in conventional seismic reflection data, without exploring the inherent illumination deficiencies of such complex structures. Since seismic imaging interpretations in both academia and industry are primarily considered in two-dimensional slices, the three-dimensional complexity of fluid pipes has not been considered in terms of how it affects seismic imaging limitations. The edge curvature of different pipe boundaries is a worthwhile angle for analysis.

To address this, we introduce a forward solution, specifically seismic modeling for illumination studies, which can significantly advance geological understanding through robust interpretation of architecture and elastic information (Laurain et al., 2004; Gjøystdal et al., 2007). This method can be used to explore the illumination conditions of different realistic pipe-like models under various survey conditions. The advantages of this approach are its speed, cost-effectiveness, and efficiency, providing geologists with powerful tools to enhance geological understanding of diverse imaging results for specific structures.

To better understand the seismic imaging in vertical pipe-like structures, we utilize ray-tracing modeling to focus on critical areas. Previous studies have applied ray-tracing based forward modeling methodologies (Sun et al., 2021; Yue et al., 2021). Inspired by the Loyal field in Scotland (Maestrelli et al., 2017) and incorporating realistic elastic properties, the purpose is to investigate how different boundary edge curvatures influence the illumination within internal areas and to identify potential shadow zones associated with illumination loss using simplified conduit models. This work highlights the current uncertainties related to imaging quality loss, as evidenced by previous studies, and proposes feasible solutions for analyzing potential causes and providing robust evidence specifically for illumination-induced reductions. These findings will enhance the interpretation of fluid pipe structures in conventional seismic data, thereby advancing the geological understanding of similar vertical pipe-like structures in comparable sedimentary environments and formation processes.

2 Geological setting and datasets

The Loyal field, located on the southern edge of the Faroe-Shetland Basin at the NE Atlantic Margin, was discovered in 1994 and extensively mapped by 1999 using 3D seismic data (Figure 1A). This basin reveals a dynamic geological and tectonic evolution (Doré et al., 1997; 1999; Dean et al., 1999; Roberts et al., 1999; Watson et al., 2017), marked by significant compressive events during the Eocene to Pliocene epochs that led to the inversion of ancient rift structures. These tectonic forces shaped the Mesozoic/Paleozoic structures, such as the Judd High, and contributed to the development of the NE-SW oriented structural highs and folds (Sørensen, 2003).

The data available for this study is a high-resolution 3D seismic dataset, initially released by BP and reprocessed in 2010 by Western Geco and CGG. This datasetcovers an area of approximately 15 × 17 km^2 (Figure 1B). Situated at the southern edge of the Faeroe-Shetland Trough channel, the seismic data are binned at 12.5 × 12.5 m^2 for both inline and crossline. The time pre-stack Kirchhoff migration technique was used to process the seismic data, where the migration was carried out in the time domain before the stacking process. The dataset includes a time-lapse survey from 1996 to 2010, with a frequency spectrum of 20–80 Hz below 4 km depth, characterized by zero-phase American polarity.

The nearby well log data (204/20-3) provides critical ties for seismic analysis and synthetic modeling, reflecting continuity with primary pipe groups in the central and southern regions (Figure 1C). The Vertical Seismic Profile (VSP) data indicates overburden velocities ranging from 1,700 m/s to 2,400 m/s (tuning thickness (λ/4) between 5 and 27 m) and densities from 1.58 to 2.00 g/cm^3, establishing foundational properties for synthetic seismic models for this research. Previous studies and geological findings (Dean et al., 1999; Sørensen, 2003; Ritchie et al., 2008; Maestrelli et al., 2017; Watson et al., 2017) suggest that the shallow part comprises shale with minor sandstone/silt content.

3 Methods

Ray tracing is a computational method used to model the propagation of seismic waves through subsurface materials (Yilmaz, 2018). It simulates the path of seismic rays as they travel from the source to the receiver, considering refraction and reflection at interfaces with varying acoustic properties. Snell's Law governs how rays bend at boundaries, based on velocity contrasts between layers. In illumination analysis, ray tracing helps evaluate how seismic waves penetrate and reflect within complex geological structures, providing insights into the distribution of illumination and identifying areas of poor seismic coverage, especially in formations like pipe-like structures.

Seismic illumination studies using ray-tracing modeling has survey design and acquisition evaluation (Gjøystdal et al., 2007). Synthetic geological models are created based on realistic and reasonable stratigraphic and structural interpretation parameters, such as horizons, interval velocities (Vp and Vs.), and density. The wavefront construction (WFC) then simulates theoretical seismic

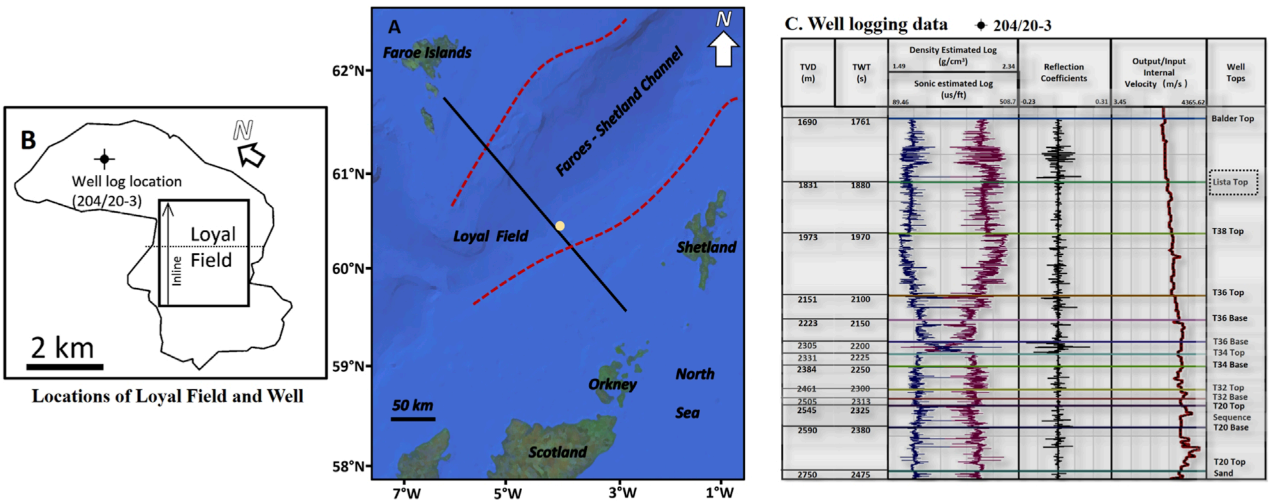

FIGURE 1
Location, seismic data, and well logging data (modified from Maestrelli et al., 2017). **(A)** The Loyal Field is located between the Faroe Islands and Shetland. **(B)** A horizontal map from the seismic dataset marks the location of an analogue well log with a yellow dot, as shown in **(A)**. **(C)** Well 204/20-3 provides essential elastic information.

waves or energy, allowing them to propagate through these realistic models (Vinje et al., 1993). The resulting ray attributes, e.g., travel amplitudes, are derived and used to create illumination maps on the target horizons. Synthetic seismic shot gathers are generated for each shot using these attributes from the survey, and a general processing sequence is applied to these shot gathers to obtain a migrated post-stack section (Figure 2).

The illumination studies performed in the present work are 3D via the generation of illumination maps, including the so-called Simulated Migration Amplitude (SMA) attribute which estimates PSDM amplitudes on a given horizon without needing to perform a full PSDM (Laurain et al., 2004). Such illumination studies allow exploring possible shadow zones and understanding amplitude variations on selected horizons. The illumination of a horizon in seismic is influenced by several factors, i.e., the possible complexity of the overburden (horizontal and vertical variability), as well as the topology of that horizon itself. Illumination analyses are able to check for undershooting situation as well, looking at the shadow zones interactively and then assessing and applying the optimized and less-costly ones.

4 Model building

The model-building process for this experiment relies on seismic interpretations derived from actual seismic images and incorporates robust elastic data to construct accurate geological models for illumination analysis (Zong et al., 2022). We use two simplified pipe models and two realistic 3D seismic synthetic volumes, with each model integrating interpreted elastic properties. For simplicity, each reflector is assumed to be entirely flat (0° dip) and accounts for only 0° incident-angle reflections. This simplifies our analysis, though it is noted that actual underground pipe structures are considerably more complex.

4.1 Seismic interpretation

The Loyal Field features a range of fluid escape structures, varying from 600 to 1,600 m in length and from several tens to hundreds of meters in diameter. These structures transition from straight columns to broader seepage areas, yet consistently exhibit typical pipe characteristics (Figure 3). Seismic imaging captures key aspects of these pipes, including internal channels, flanking boundaries, fluid-rich bypass areas, and the terminus and roots. Although the overall shapes of the pipes remain visible, the seismic signals from these structures tend to be weak and chaotic in internal conduit areas due to possible imaging quality loss, making it difficult to discern detailed geological features. In the subsequent forward modeling work, Pipe I is assigned to simulate P3 and Pipe II to simulate P1, allowing to obtain synthetic seismic models of pipe structures that are closer to the real scenario.

The pipe anomalies exhibit various architectures in 2D above, as observed in several realistic consecutive time slices. But these variations in 2D reflect the even more complex nature of their 3D structures (Figure 4). The changes seen across these time slices indicate that the geometries and internal characteristics are not only diverse but also evolve in ways that are intricate and multifaceted when considered in 3D. This complexity highlights the challenges of interpreting such complex features using 2D seismic data alone.

4.2 Geometric model

In this study, we developed two simplified geometric models for illumination analysis: Model I for Pipe I and Model II for Pipe II, as shown below.

(1) In Model I, we explore the effects of boundary structure on internal dynamics and illumination loss using a simplified boundary conduit model. To accurately simulate real-world

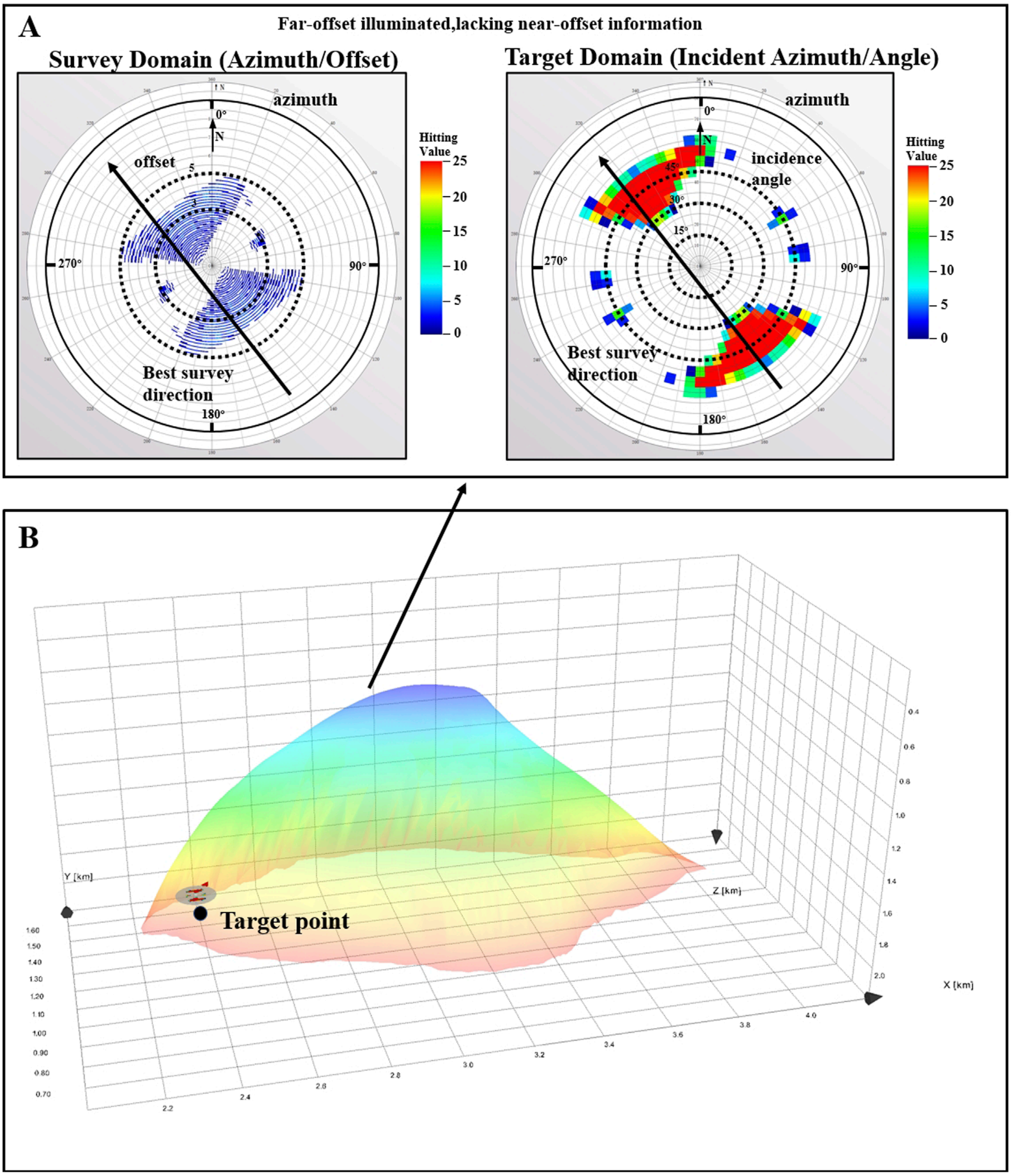

FIGURE 2
(A) Flower plots illustrate the illumination on a specific subsurface target point located on the boundary of a pipe conduit. These plots represent the azimuth and offset (in the survey domain) or the incident azimuth and dip angle (in the target domain) of reflectors that are potentially illuminated by a particular survey. Two types of flower plots are included: one for the survey domain using azimuth and offset, and another for the target domain using azimuth and incident angle. Target points **(B)** can be any location within the 3D subsurface work area.

pipe architectures, we selected specific pipe numbers and developed geometric models. These models consider variations in the sizes and irregularities of conduit boundary shapes, featuring different radii (0.94 km and 0.33 km) and curvature at the boundary edges. The conduit is conceptualized as a wrapping surface around the pipe structure, effectively representing a typical pipe configuration. The model details, as illustrated in Figure 5A, show a pipe body that is 1.36 km tall

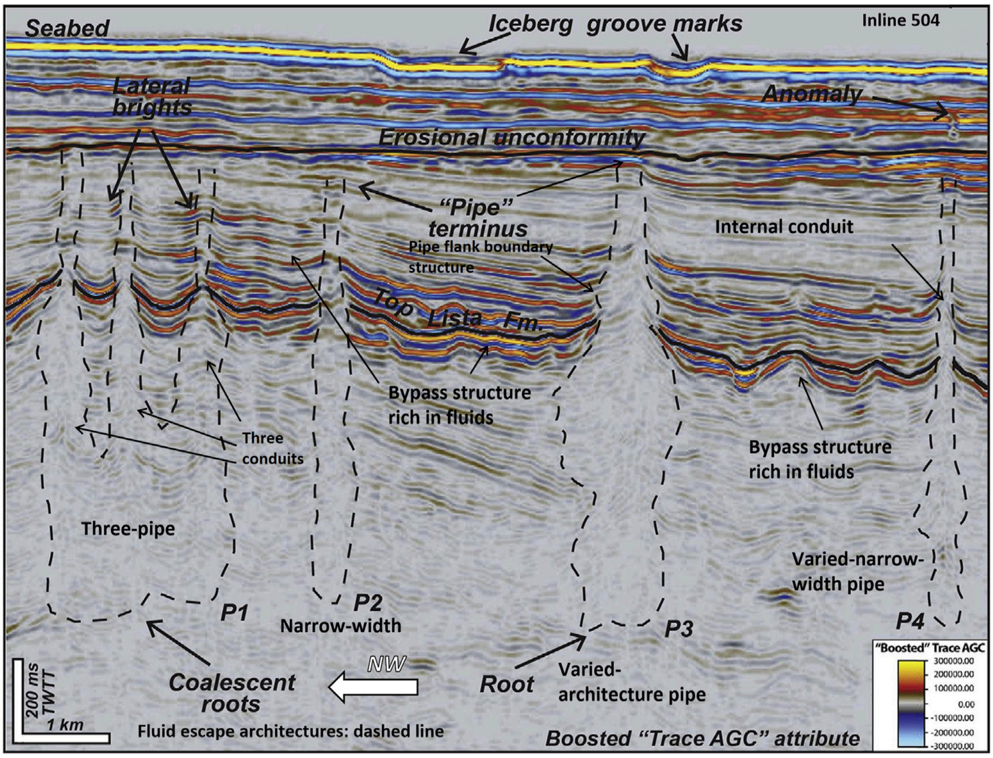

FIGURE 3
An inline seismic section from the Loyal field illustrates the diverse structures of fluid escape pipes (modified from Maestrelli et al., 2017). "Boosted" Trace AGC is used to enhance amplitude contrast and improve resolution in areas of low clarity. This section reveals individual (P3) and interconnected (P1) pipes, presenting the diverse architectures of this vertical and complex shallow structure.

with long and short radii of 1.7 km and 0.76 km, respectively. On one side of the pipe body, a gradient trend in the boundary flank is observed, with high and low curvature at different edges. This irregular shape enables the exploration of how internal illumination distribution varies with different internal locations, applicable to various shapes of pipe-like seal bypass conduits and potential shadow zones. Furthermore, we consider different internal intrusion velocities to simulate both unconsolidated and dense internal conditions, allowing for an exploration of seismic illumination variations across scenarios with low, lower, and high internal velocities (Figure 5B). Moreover, this model also features varied edge curvatures at the top layer of the conduit structure. To assess the impact on seismic illumination, selected illumination point groups for the Boundary Outside (BO, outside area of the boundary structure) and Boundary Inside (BI, inside area of the boundary structure) are positioned along the boundary flank at different curvature edges (Figure 5C). This arrangement facilitates a qualitative analysis of seismic illumination in relation to the internal velocity characteristics of the pipe structures.

(2) Model II is designed to further investigate the seismic illumination and shadow zones at the root areas of pipes. This model simplifies the structure by reducing the number of conduit layers from approximately 14 to just 4 (Figures 6A, B). Velocity fields for Pipe I and II are presented to enhance visualization (Figures 6C, D). Elastic parameters details the elastic property parameters of pipe structures for different model scenarios. This reduction facilitates the penetration of rays through the conduit layers, aiming for optimal illumination results. This model is the simplified version retaining their critical components, particularly the vertical pipe boundary features and the conduits. The target root layers are specifically assigned at the rooting parts of the pipes.

4.3 Elastic parameters

We have derived key elastic parameters—P-wave velocity (V_P), S-wave velocity (V_S), and density (ρ)—from well-log data in the Loyal field. These measurements are secured by extensive literature and regional geological surveys from the Faroe Basin to Shetland, providing a robust framework for our seismic models (Maestrelli et al., 2017; Watson et al., 2017). Models I and II are both divided into different layers, with their properties detailed in Table 1. We particularly focus on small-scale pipe structures, where amplitude strength profiles suggest notable impedance contrasts being used to guide realistic V_P and density for our simulations (Zong et al., 2023; Sun et al., 2024). V_P ranges from 1.6 to 2.5 km/s. Poisson's ratio (σ), ranging from 0 to 0.5, helps ascertain the fluid content in sand and shale formations, influencing the V_P/V_S ratios essential for V_S determination (Mavko et al., 2009), as shown below:

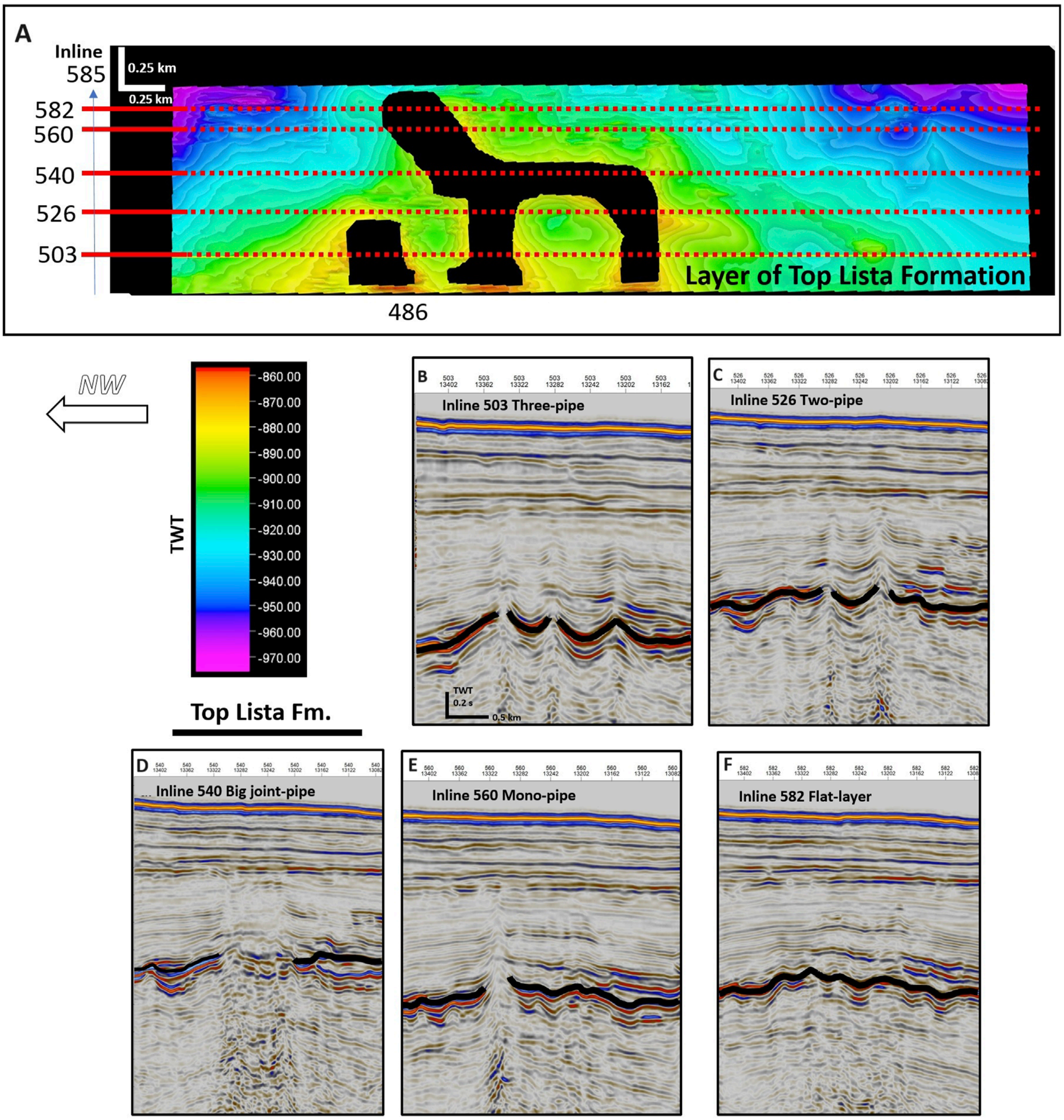

FIGURE 4
Seismic images reveal fluid escape pipes, such as Pipe II, from "Boosted" Trace AGC sections within 3D seismic PSTM volume (P3 in Figure 3; Pipe II). **(A)** The horizontal distribution is mapped by the Top Lista Formation, displaying five sections: **(B)** 503-three-pipe, **(C)** 526-two-pipe, **(D)** 540-big-joint-pipe, **(E)** 560-mono-pipe, and **(F)** 582-flat-layer, with black arrows indicating various shapes. This 3D pipe architecture exhibits numerous limitations when observed in 2D slices, showing a range of different appearances.

$$\frac{V_p}{V_s} = \sqrt{\frac{2(1-\sigma)}{(1-2\sigma)}}$$

Density is determined using a formula that is slightly adjusted according to the lithological characteristics. The Vs is derived using a ratio that ranges from 1.6 to 3.05, reflecting variations in fluid content. Density is derived from V_P based on the rock type. The AI values (V_P*density) relative to the amplitude distribution are utilized to delineate surrounding lithological characteristics.

5 Result

5.1 Flower plots

A simplified 3D pipe model is constructed as Model I, featuring various curvatures at the top layer edges of the conduit structure. Selected illumination point groups are strategically placed along the boundary flank at these differing curvatures to study the

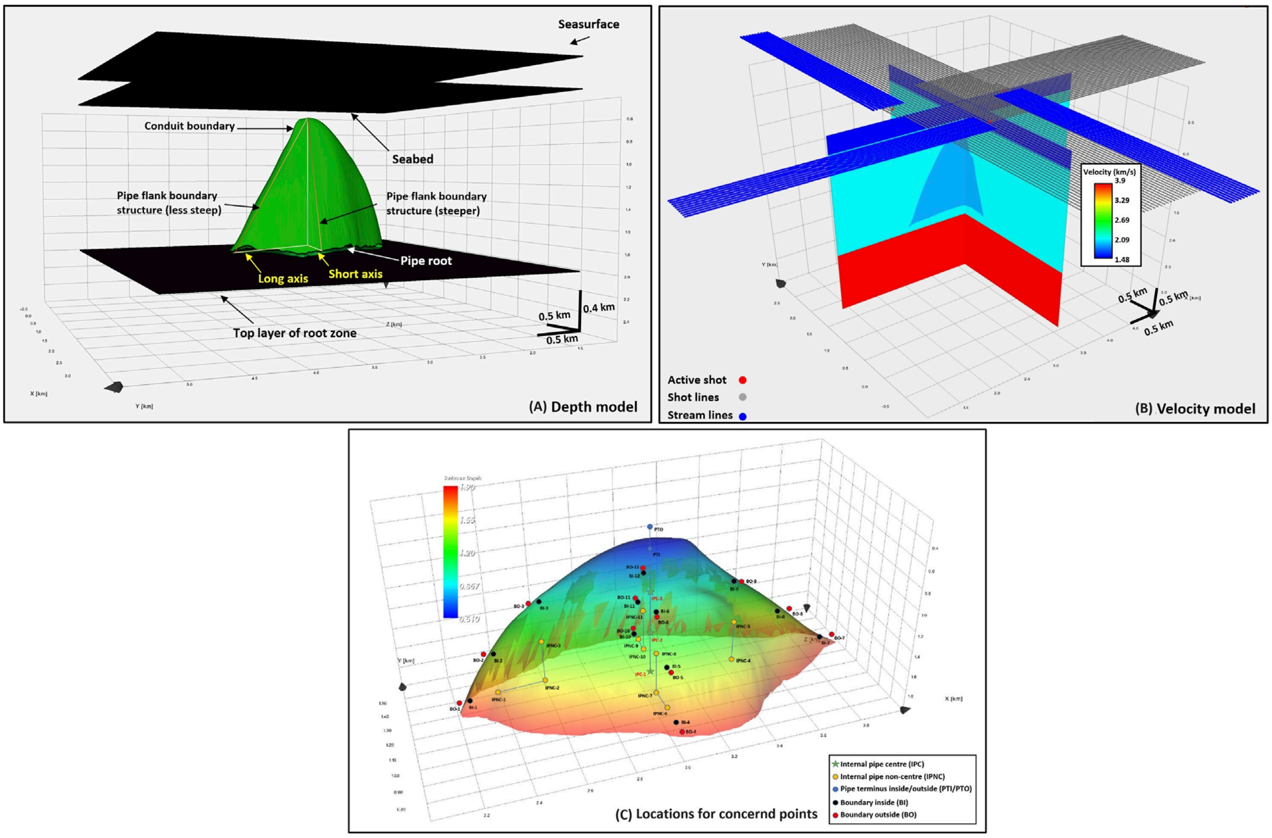

FIGURE 5
Simplified 3D depth and velocity models are used to highlight various diameters, boundary curvatures, and flank gradients, along with key point locations. **(A)** The depth model outlines a pipe conduit boundary with a specialized shape, creating flanks with different curvatures. **(B)** The velocity model shows velocity distribution and survey geometry in four directions. **(C)** Illumination points in this simplified low-velocity pipe structure areas are identified produced, aiming to be assessed how the boundary wall affects illumination loss, focusing on edges with different curvatures. Cared points for both outside (BO) and inside (BI) boundaries will further been produced flower plots of illumination in the survey and target domains.

impact on Boundary Outside (BO) and Boundary Inside (BI) areas, as well as the formation and effects of shadow zones. This experiment allows for a detailed examination of how boundary shapes and their curvatures influence internal visibility, illumination distribution. Figure 7 presents a series of flower plots illustrating the illumination conditions for points located both inside and outside the boundary structure, across regions of low and high curvature edges. This visualization aids in comparing the illuminated offset span in the survey domain and the illuminated incident-angle span in the target domain. The results highlight a significant reduction in illumination within the internal conduit areas due to the obstructive boundary wall. Notably, illumination decreases substantially along the flanks of the boundary, particularly at steeper curvatures, indicating increased light loss within these internal areas.

5.2 Edge curvature

The curvature of the 3D edge is important in assessing whether surfaces are on-head (perpendicular to the boundary surface), as depicted in Figure 8. The results illustrate that varying curvatures of the pipe boundary significantly influence the illumination coverage within the internal areas of the pipe conduit. Specifically, higher edge curvatures enhance the illumination levels adjacent to the inside boundary, likely because these curvatures facilitate greater ray penetration and subsequent convergence in narrower areas. The illumination offset range tends to follow a trend similar to the tangent of the edge curvature, as indicated by the forms of illumination dip shown in Figure 8A. While far offsets receive illumination, the near to middle offsets experience minimal coverage due to a scarcity of head-on illuminated rays. On the other side, with a smaller curvature of the pipe edge (Figure 8B), the inside boundary locations do not converge penetrating rays into a smaller area but can receive more head-on rays, enhancing illumination along the diameter direction. However, the trend remains that the relatively inner areas are primarily illuminated by far offsets, with the near to far offset ranges better illuminating areas closer to the boundary surface. This pattern may be due to the high flank gradients of the boundary, which prevent vertical rays from being received by horizontal-reflector points.

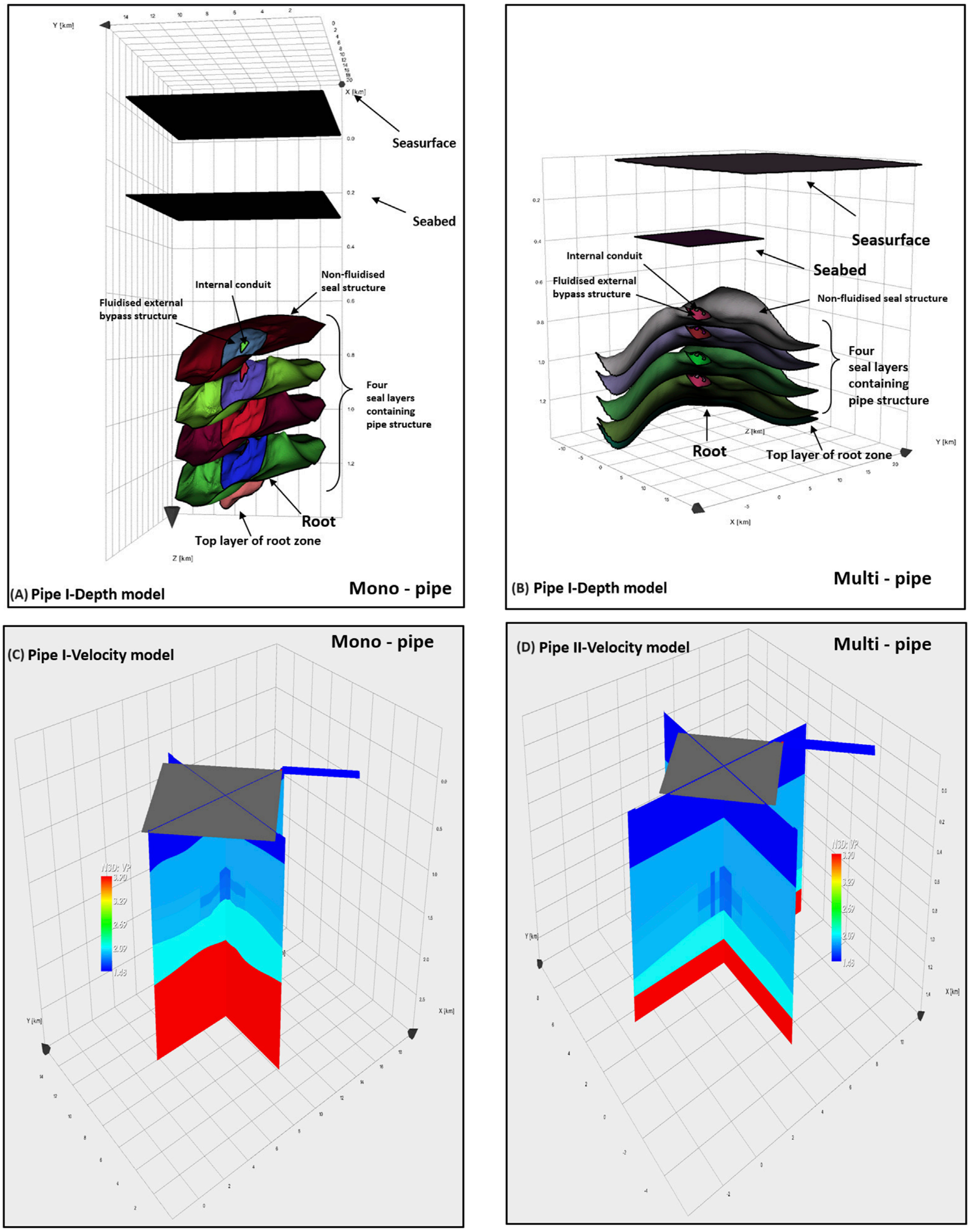

FIGURE 6
Simplified 3D depth **(A, B)** and velocity models **(C, D)** based on interpreted Pipe I **(A, C)** and Pipe II **(B, D)** are shown for SMA illumination analysis. These models are simplified versions of Model **(I)**. The vertical scale is significantly exaggerated to enhance visibility, although it introduces slight surface fluctuations.

TABLE 1 Elastic property parameters for Model I and II. The values are all assumed by thoughts of combining empirical formulas, previous seismic interpretations, the geological setting and the amplitude strength from the real seismic profile, aiming to reach the most realistic level. All relationships are based on Mavko et al. (2009).

Lithology		V_P (km/s)	Average Poisson's ratio (σ)	V_P/V_S	Density (g/cm^3)
Basic information for Model I and II	Layers other than pipe conduit	1.6–2.5	0.404	2.5	1.75 $Vp^{0.265}$
	Bypass structure rich in fluids	1.8–2.5	0.3	1.87	1.6 $Vp^{0.265}$
	Internal conduit	1.807	0.404	2.5	2.047
	Sediment (outside internal)	2.1	0.404	2.5	2.2
Additional information for Model II	Low	1.9	0.3	1.87	2
	Lower	1.73	0.3	1.87	2
	High	2.5	0.3	1.87	2

5.3 Shadow zone

We use Model II to investigate shadow zones within the pipe structures, which features two simplified yet realistic pipe geometries. These models are equipped with appropriate geophysical inputs to facilitate illumination studies under specific survey geometries. Using the Seismic Modeling Approach (SMA), the horizontal layer at the pipe root areas is analyzed, providing a visualization of horizontal illumination variations at this level, which is critical for understanding the low-illumination shadow zones associated with weak seismic amplitudes.

Figure 9 delineates a distinct lack of SMA strength within the pipe root areas. In the mono-pipe scenario (Figure 9A), the horizontal illumination distribution clearly delineates the root areas from the fluid-rich bypass structures and non-fluid-bearing sealing layers. The shadow zones, marked by extremely low illumination levels, are identified beneath the main internal pipe conduit. These areas exhibit particularly poor illumination due to the suboptimal engagement of survey geometries. In the more complex multiple-pipe scenario (Figure 9B), a similar pattern emerges, with clear shadow zones due to the variable boundary conditions and irregular geometrical formations. The sensitivity of these structures to survey direction is highlighted, particularly when exposed to steep vertical boundaries, which significantly obstruct wave energy, creating focused shadow areas. Nevertheless, this obstruction is mitigated when the vertical boundary surfaces are narrower, allowing for better ray penetration.

Thus, the shadow zones elucidated in this analysis underscore the substantial illumination loss attributable to boundary structure walls. In fluid-rich bypass areas, high hit counts suggest robust illumination, potentially indicating the presence of multiple seismic reflections, though this hypothesis warrants further investigation. Additionally, significant illumination is detected beneath the boundary conduit parts, as evidenced by high amplitude responses along the survey direction. This phenomenon suggests that the shot source side may contribute to increased amplitude signals at the layer surface beneath the overburden sealing structure. The observed high amplitudes at boundary parts suggest enhanced illumination coverage, likely influenced by high impedance contrasts. However, if the pipe conduit area is extensively large, the illumination could be significantly diminished or remain at the far offsets. This peculiar high illumination could lead to amplitude artifacts at the root parts of the pipe, particularly at the boundary edges, offering a potential explanation for the chaotic nature of central root parts.

6 Discussion

6.1 Pipe boundary

6.1.1 The main contribution to illumination loss

The pipe boundary flank is a critical factor to consider as it could impact the internal illumination of the pipe. The findings suggest that a steep boundary flank is more effective in preventing raypaths from entering the pipe body at the closest locations. Therefore, this study postulates that a steep flank boundary structure, accompanied by certain lithological differences, is the primary contributor to the loss of internal illumination. This partially supports previous studies that the pipe boundary exhibits transitional areas between reflection continuity of the outer layer and seismic discontinuities within the interior (Løseth et al., 2011). In most pipe cases, the central areas usually have a highly sharp boundary structure, resulting in extremely poor internal-boundary illumination conditions, leading to further poor imaging quality.

6.1.2 3D boundary edge curvature

The 3D columns of pipe features are generally irregular and formed by different materials due to upward pressure, such as volcanic mudstone, salt, hydraulic flux and gas eruption (Cartwright et al., 2007; Davide et al., 2021; Hansen et al., 2005; Judd and Hovland, 2007). Generally, the internal structure can experience different surrounding sedimentary environments and producing a mixture of multiple parts (Maestrelli et al., 2017). Different boundary flank shapes of subsurface pipe-like targets thus display enough variation and diversity (Cartwright and Santamarina, 2015; Løseth et al., 2011).

The results of the 3D illumination study of pipe boundary structure suggest more detailed and advanced illumination

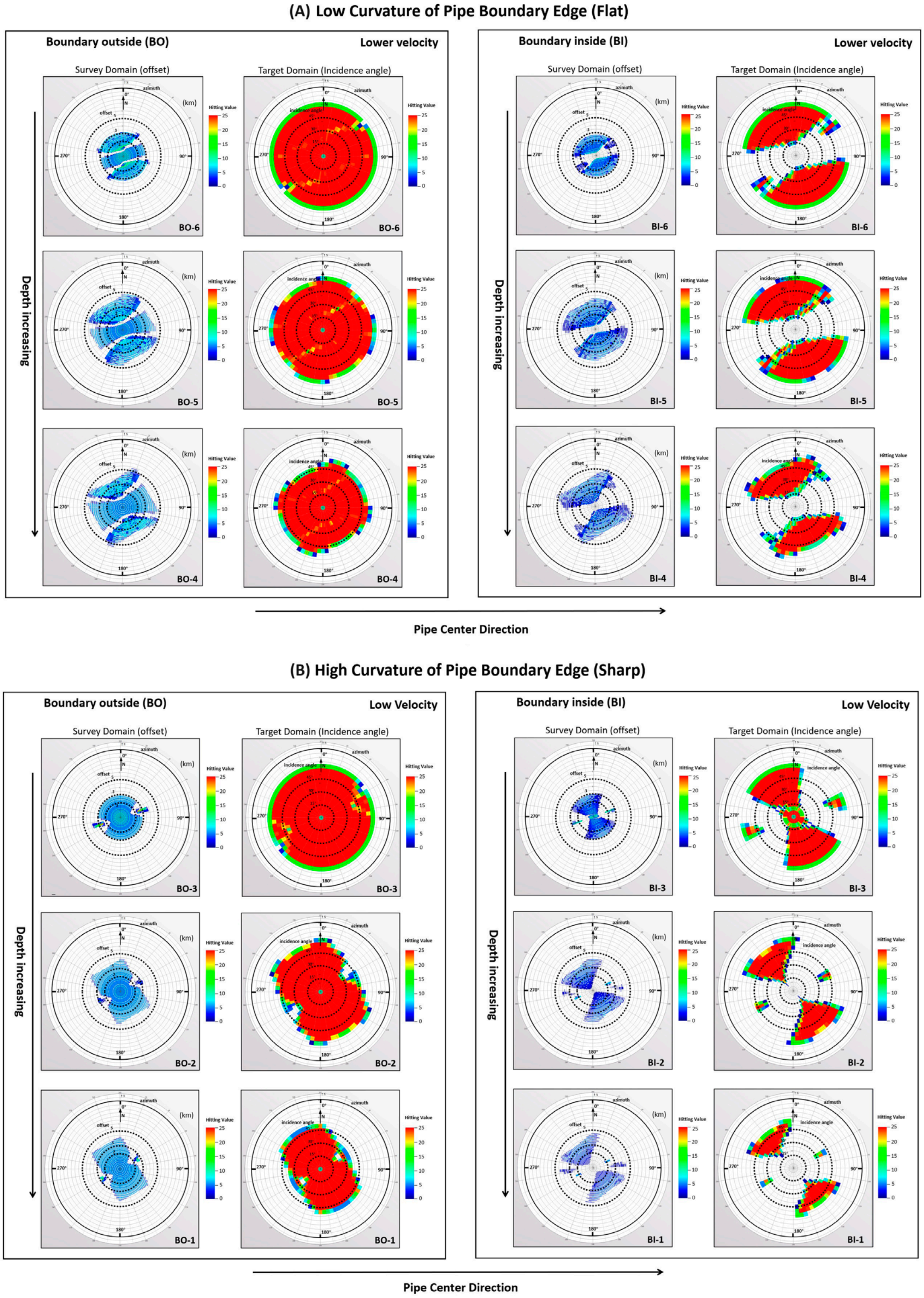

FIGURE 7
Flower plots for low and high curvature of pipe boundary edge of Model I within internal low velocity produced by 3D survey-independent ray tracing. Boundary outside structures illustrate relatively high illumination status. **(A)** Low curvature shows that the internal boundary locations present strong far-offset illumination but very weak in near-offset with the direction perpendicular to the diameter. **(B)** High curvature presents the similar trend with the internal location conversely showing direction parallel to the diameter.

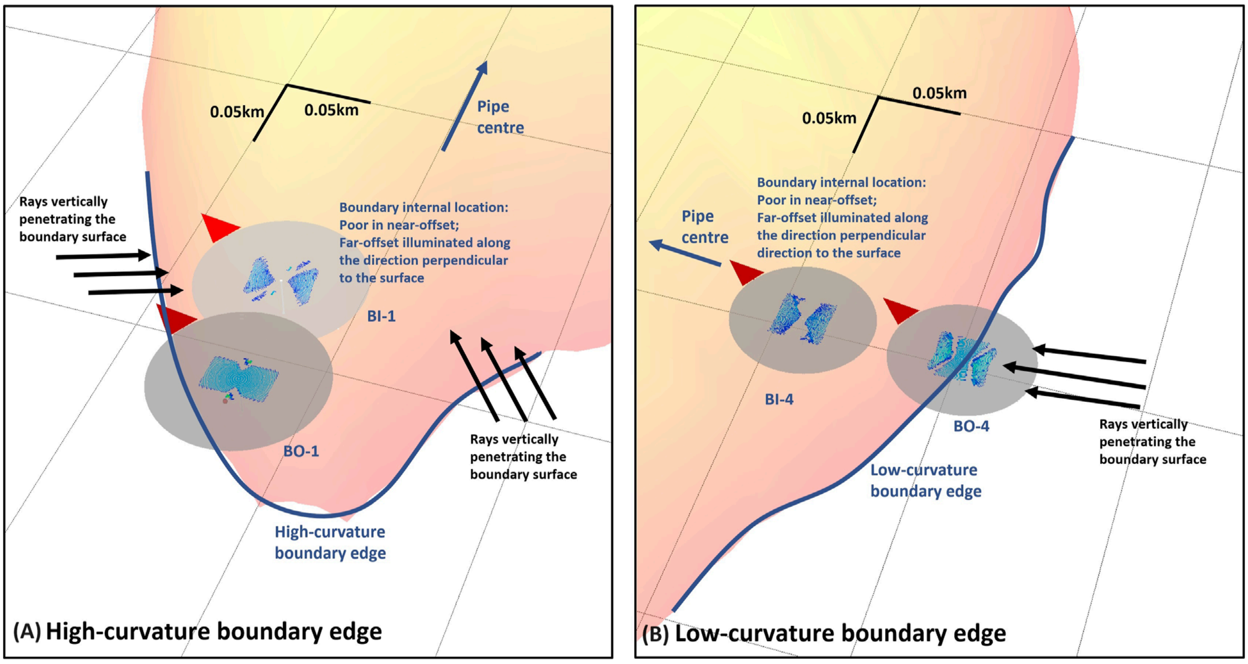

FIGURE 8
Illustration diagrams for ray penetrating the boundary surface based on high and low curvature boundary edges thus causing different illuminations of boundary internal locations. Boundary internal locations show poor illumination in near-offset, along with far-offset illuminated. The internal one with **(A)** high- and **(B)** low-curvature sides present different illumination directions as perpendicular and parallel to the diameter direction respectively.

conditions than that of 2D, which offer more authenticity. As shown in Figure 10A, it is important to recognize areas receiving perpendicular rays to the boundary surface exhibit substantial illumination improvements. Despite this, the general illumination of the near offset is nearly extinguished across all survey directions, underscoring the profound effect the boundary wall has on light penetration into the internal structure of pipe-like formations with low velocity. Moreover, the results suggest that higher curvature means bigger angle coverage around its central point within a given line segment, i.e., more sharpness of the edge corner. The results also show that sharper boundary edges resist a significant amount of penetrating rays along the diameter axis at near-offset range, but not at the almost contact internal location. However, the orthogonal direction can receive high levels of illumination effects at far-offset. In contrast, lower curvature edges, i.e., less sharp and flatter boundary surfaces, present high illumination along the diameter axis with the direction parallel to the boundary surface. This situation typically occurs when considering only a short distance from the boundary interface to internal points. As the overall illumination gradually increases, the distribution of illumination becomes more even in both azimuth and offset. This finding demonstrates that boundary structures critically influence internal visibility in seismic imaging, impacting the overall effectiveness of illumination in these geological settings.

This study is the first to attempt 3D illumination analysis of subsurface pipe-like features by considering the 3D architecture of boundary structures. Previously, the focus was more on 2D sections because industrial applications mainly concentrated on interpreting 2D slices (reference). This might be due to the fact that interpreting 3D volumes is relatively more expensive, time-consuming, and less cost-effective for later reservoir identification. However, 3D analysis can reveal aspects that 2D perspectives cannot, such as the varied 3D boundary effects, which are particularly important for highly complex pipe-like structures.

6.1.3 Geophysical explanation

This work assumes that the main factors causing poor illumination coverage are the high velocity impedance contrasts and the extreme vertical wall shape between the internal and boundary conduit areas. The boundary barriers might cause up to much signal loss in two pipes in this illumination analysis. This may attribute to the vertical-shape boundary wall with high impedance contrast, along with potential anelastic and scattering attenuations induced by the fluid-bearing conduit (Cartwright and Santamarina, 2015; Løseth et al., 2011).

The main reason for the illumination loss is likely the obstruction of raypaths by the boundary structures. Based on the Snell's law in geophysics (Yilmaz, 2018), downgoing raypaths penetrating the boundary surface will be hugely bent by the higher extent of velocity difference. Figure 10B shows that due to the high velocity of the boundary conduit and the much lower velocity of the internal pipe, only rays shot with narrow offsets can be reflected by the internal layers. As a result, the effective shooting range coverage is greatly reduced at the sea surface with survey layout, resulting in significant illumination loss in the internal pipe areas. The results suggest that internal areas closer to boundary structures are more likely to experience greater energy loss impact. As shown in Figure 11A, when approaching the boundary areas,

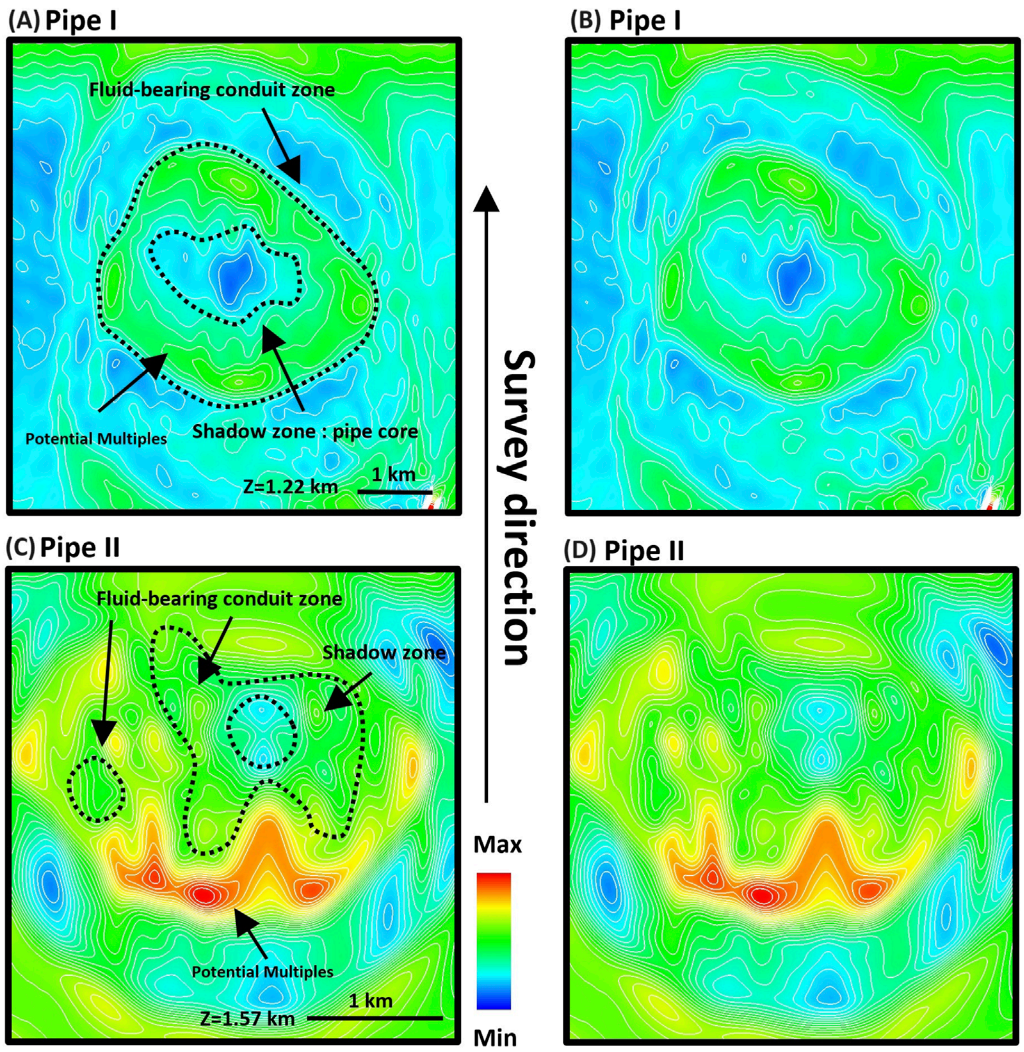

FIGURE 9
SMA illumination maps for flat horizontal bottom target below root parts of two simplified pipe geometries resembling **(A)** Pipe I and **(C)** II in Model III. See **(B)** and **(D)** for the clean images. Underneath parts within pipe boundary areas containing more ray hits (from outside normal impedance contrast layers) along survey direction, possibly due to the fluid-bearing high impedance contrast sealing sequences, thus forming potential multiples. The horizontal shadow zone can clearly illustrate very weak horizontal illumination of corresponding pipe structures. The dashed lines represent self-defined boundaries on the cross-section, delineating the internal pipe region (inside the dashed lines) and the external boundary areas (outside). The space between the two dashed lines defines the boundary areas.

reverse ray paths indicate that rays with overly critical incident angles from the surface cannot reach these regions, thus explaining why these areas fail to receive rays that penetrate the upper boundary and are illuminated along one-way ray paths. This also suggests that larger velocity differences result in larger coverage of upper parts precluding effective rays for the inside boundary locations. From the perspective of ray paths, this reveals possible reasons why locations inside the pipe closer to the boundary interface have weaker illumination, i.e., fewer effective rays.

From another perspective, Figure 11B examines that internal-pipe target locations farer to boundaries may reduce the illumination-failure coverage on the upper pipe parts, which means more acceptance rates of effective rays. In other words, narrow pipes may not be able to fully cover the internal low-level boundary areas, resulting in signal loss. This is particularly apparent and important for some extreme vertical pipe boundary structures, e.g., 1,000 m blow-out pipes (Løseth et al., 2011). Pipe internal structures may then have further imaging quality improved by using wider azimuth and offset (Cartwright and Santamarina, 2015). Larger pipe can allow more rays to penetrate the internal layer interfaces then reflected, thus the major central pipe parts being less interfered because of wider-offset rays received from the upper pipe section without boundary interface effects. It should be also noted about the vertical resolution of ¼ λ, however it seems very little impact even with input as high velocity of 2,500 m/s and low frequency of 10 Hz then resulting for 62.5 m. This conforms to what (Moss and Cartwright, 2010) claimed as pipe diameter over 100 m will not involve any problems of vertical resolution.

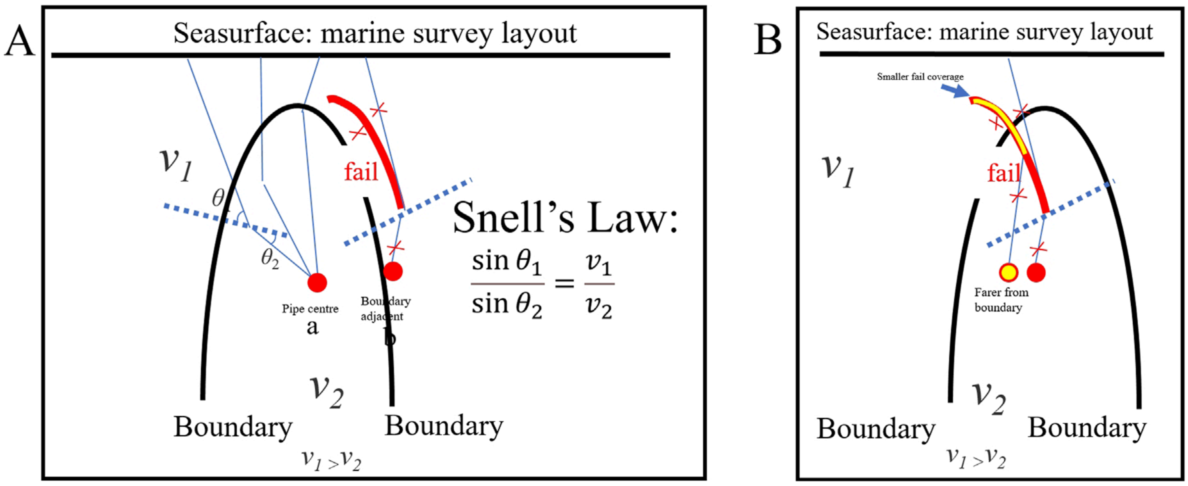

FIGURE 10
Illustrative diagrams for rays penetrating the boundary surface of pipe structure with angles of 90° (perpendicular) and some incident angle. **(A)** Rays of can allow more wave energy going inside with the least energy loss, thus providing more illumination. **(B)** Rays of right will induce some wave energy loss of rays after transmission, causing some illumination loss. The illumination coverage of internal structure in condition **(A)** with 90° incidence rays is less than that of condition **(B)** with incidence rays less than 90°.

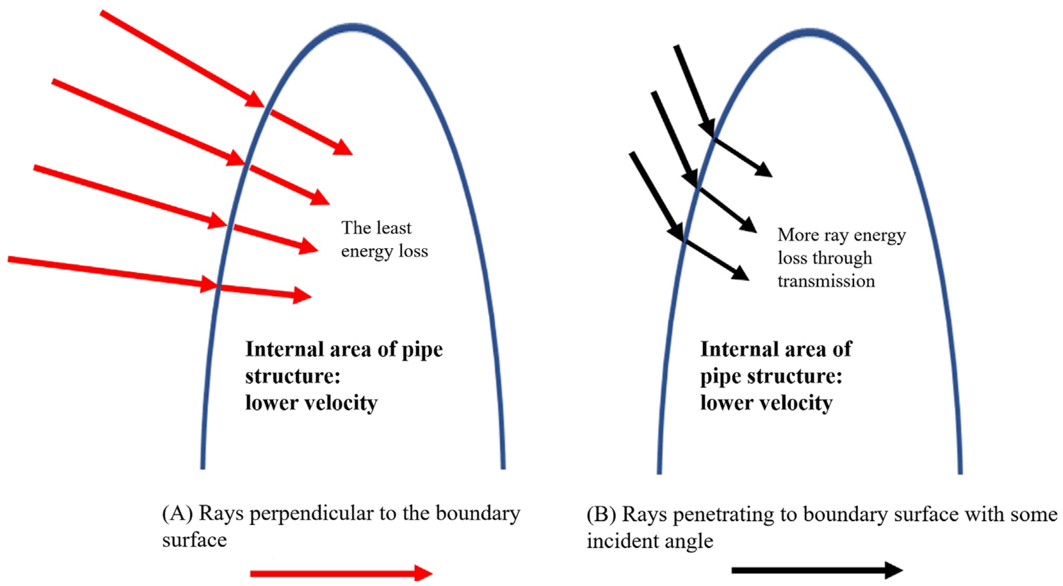

FIGURE 11
(A) Simple illustration diagram presenting the failure illuminated raypaths due to the close distance to the boundary structure. Rays reaching the pipe centre, as in **(A)**, can follow Snell's Law to pass the boundary interface with rays bending. The red areas may be the failure areas for rays starting from **(B)**, causing over-bending and then over-critical incidence. **(B)** Simple illustration diagram presenting the failure illuminated raypaths for different distances to the same boundary interface. At the same depth, a greater distance from the boundary interface results in less failure illumination coverage, shown as yellow points and line segments.

6.2 Shadow zone

Shadow zones, or low-illumination areas, refer to subsurface regions that lack essential seismic waves or exhibit minimal seismic reflection activity (Nanda, 2016). The results suggest that this phenomenon is likely due to the partial absorption of energy. Illumination loss within the internal pipe structure can lead to the formation of shadow zones, creating potential narrow areas of illumination. This typically occurs in the shallow subsurface when seismic waves are distorted by abrupt structural changes or extreme elastic variations, resulting in reduced and degraded wave energies. In the context of vertical pipe-like structures, this study, supported by the 3D illumination analysis, has identified potentially several areas containing shadow zones.

Based on the above analysis, a 3D diagram of a typical pipe-like structure, including shadow zones, is proposed (Figure 12A). The results indicate that for vertical pipe-like structures with lower internal velocity, the shadow zones are primarily located along the inward boundary areas and the bottom regions (see top layer of root zone in Figure 5A), including the root parts beneath the boundary conduits and the main sections of the pipe bodies. This suggests that the internal structures of the pipes exhibit poor illumination, which slightly improves towards the adjacent boundary areas. The illumination is weakest in the internal regions of the pipe bodies, with a relative enhancement as one moves toward the pipe center. Additionally, there is also a brief definition of five distinct levels of illumination, each corresponding to important sections of the pipe structures, through a reasonable interpretational inference based on the results of illumination analysis. This might help to categorize the varying degrees of illumination exposure that different parts of the pipes receive.

This work has clearly identified a significantly wave-weakened zone along the internal steep flank of the pipe boundary. The results suggest that this phenomenon is primarily due to the presence of fluid conduits that absorb wave energy, combined with high velocity contrasts, steep boundary shapes, and the sharpness of 3D edges. Furthermore, fluid-saturated sealing layers and the internal structure of the pipe impair seismic energy, creating distinct horizontal shadow zones near the root areas. In regions far from the pipe body, where fluid-bearing seal boundary structures are absent, illumination coverage is further reduced. This finding supports what Løseth et al. (2011) have proposed, with their modeling results, that the boundary transition areas has massively signal loss, as well as the boundary chaotic features from other pipe-like structures with low-velocity internally (Cartwright et al., 2007; Hansen et al., 2005; Løseth et al., 2009; Petersen et al., 2010).

6.3 High hit count (multiples?)

We thus hypothesize that there may be a high hit count below the external sealing layers outside the root areas. This partially fails to fully illuminate the internal pipe roots. This work assumes that the seal layers structures (rich in fluid) create a barrier causing high hit count underneath, resulting in higher signals laterally than in the root and outside fluid-flowing areas (Figure 12B). The complex boundary of the root inhibits the passage of a significant amount of ray energy, similar to the boundary situation of the central pipe part. The speculation that this high hit count exists supports the notion of an extremely poor illumination strength of pipe features.

According to the results of illumination studies, despite the twisting and crowding of rays, there is still evidence of a large amount of wave penetration with low incident angles, i.e., wider azimuths. The wave-impairing and low signal-to-noise ratio aspects may be due to the external layers. They may strongly reflect more rays, leading to possible internal multiples and a reduction in wave energy, which may fail to enter inside in large amounts. This implies that the fluids within the external sealing structure may also act as an impediment zone that prevents potential wider-azimuth ray paths from reaching the surface geometry. It is then natural and logical to suggest that the pipe root parts can be better illuminated by a strong narrow azimuth survey, while rays from the conduit parts may be unreliable.

Pipe-like structures may occur seismic artefacts such as complex multiples (Cartwright and Santamarina, 2015). The horizontal synthetic PSDM results by SMA suggest a high number of seismic signals in this area, which may be potential multiples. However, further verification is needed.

6.4 Comparison with real seismic images

In this study, we compare our results with synthetic pipe models generated from real seismic images of the Loyal field to assess the impact of illumination on the flank boundaries of fluid escape pipes (Figure 13). This comparison reveals a similar illumination trend, providing robust validation of our ray-tracing methodology against real field data. This highlights the importance of illumination as a new perspective for understanding imaging quality loss in relation to this structure. Furthermore, an examination of the seismic details of the real seismic images, processed both with and without AGC, reveals significant quality loss in regions near the pipe boundaries. We attribute this loss primarily to a reduction in illumination, likely caused by the impact of the flank structure on ray propagation. This issue appears to be largely independent of resolution settings (Figure 14). However, for the findings related to the 3D boundary edge curvature and shadow zones, more complex 3D interpretation work is required to make similar comparisons. These results can still serve as a foundation for future research to further explore and investigate these topics.

6.5 Why illumination?

This study introduces a new perspective for seismic imaging interpretation, with a focus on illumination, particularly for vertical pipe structures or other complex vertical targets. It provides novel but important insights for seismic interpreters regarding the imaging quality loss associated with these types of targets (Moss and Cartwright, 2010; Løseth et al., 2011; Cartwright and Santamarina, 2015). We emphasize the importance of illumination in seismic imaging quality, especially in the context of ray-tracing-based methods. Such approaches are crucial for understanding the uncertainties in seismic imaging details of complex structures, as illumination effects have often been overlooked in many cases (Moss and Cartwright, 2010; Løseth et al., 2011). Similar ray-tracing methods have been applied to other targets, such as salt bodies (e.g., Jones and Davison, 2014) and faults (e.g., Botter et al., 2017), but have not yet been utilized for pipe structures. This represents the key innovation of our work. Our findings provide a new perspective for future research in seismic interpretation, offering an effective approach to reduce uncertainties in the imaging and interpretation of complex geological structures, which are common in industry-standard seismic profiles.

7 Conclusion

This research integrates ray-tracing modeling for illumination studies with high-resolution seismic and well data to enhance our

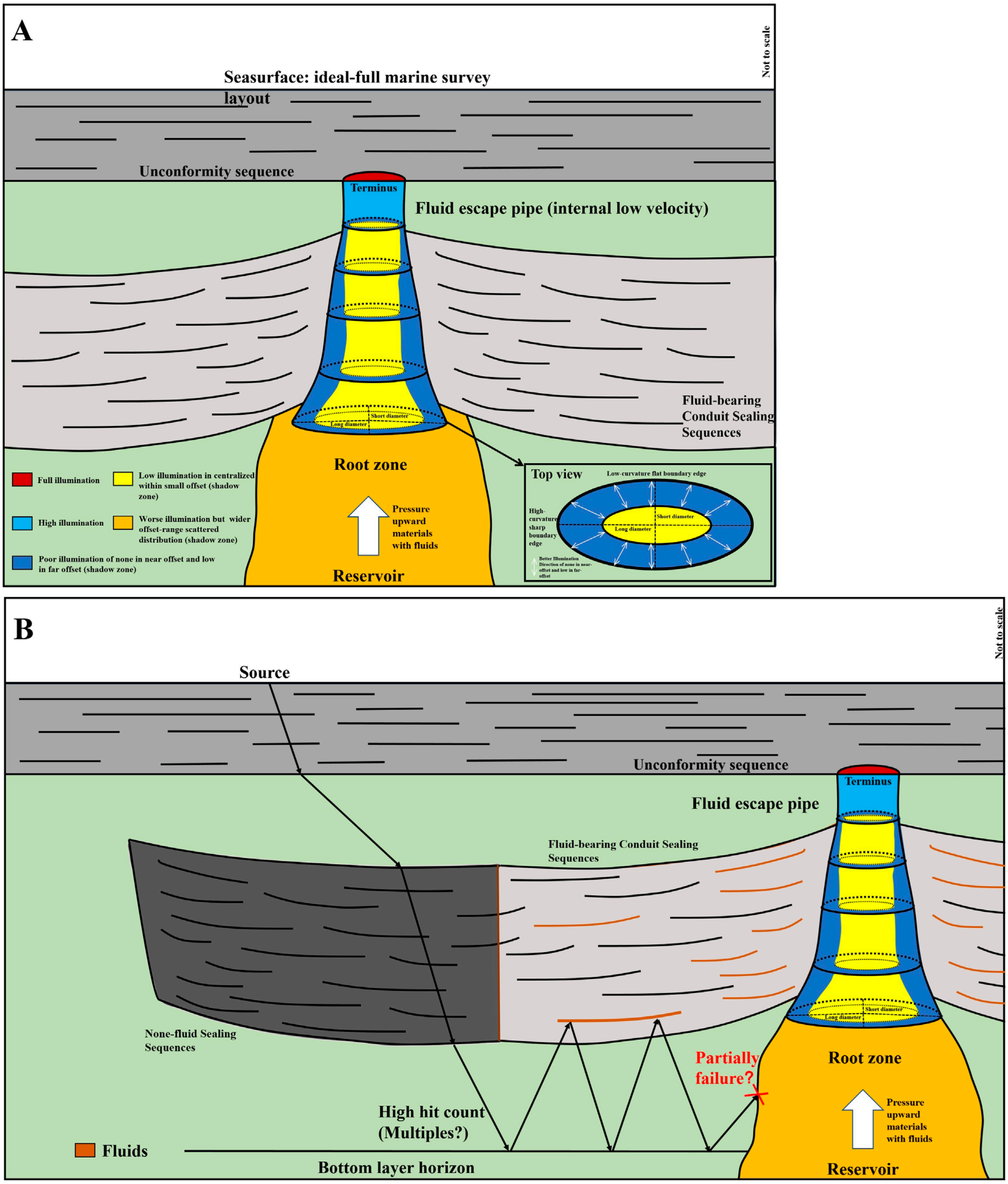

FIGURE 12
(A) Illustration diagram for the shadow zone distribution on vertical pipe-like structure within low internal velocity. Shadow zones are located at the internal boundary structures, internal pipe parts and root areas. Upper parts such as terminus and the top parts can have high illumination. The internal boundary shadow zone shows far-offset illuminated perpendicular to boundary surface. Five levels of illumination are briefly defined for different parts of the pipe structures. **(B)** Illustration diagram for underneath root areas of vertical pipe-like structure. Rays shot from outside surfaces above normal impedance contrast layers may penetrate the adjacent root parts then form high hit count (multiples?) due to the fluid-bearing high impedance contrast sealing sequences.

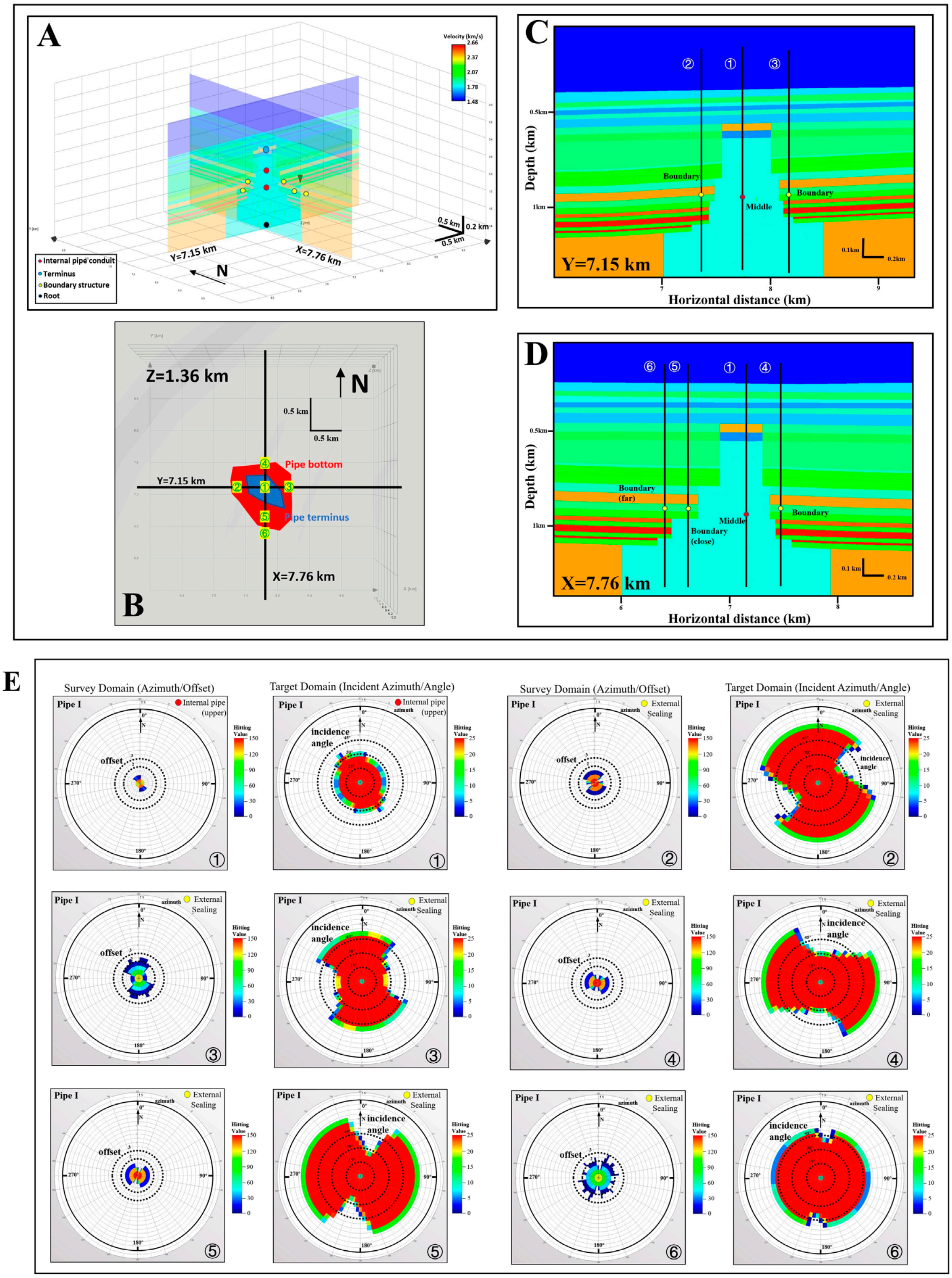

FIGURE 13
3D visualization of seismic synthetic models of Pipe I. **(A)** 3D representation of synthetic sections highlighting the key parts. **(B)** Top view of synthetic sections with important section slices and points. **(C)** X-view synthetic sections showing important section slices and illumination points, **(D)** Y-view synthetic sections displaying important section slices and points. **(E)** Illumination status near the boundary areas of the pipe, illustrating that the illumination decreases as the proximity to the boundary increases, both inside and outside the boundary. This trend is consistent with the illumination distribution observed in the previous simplified pipe model.

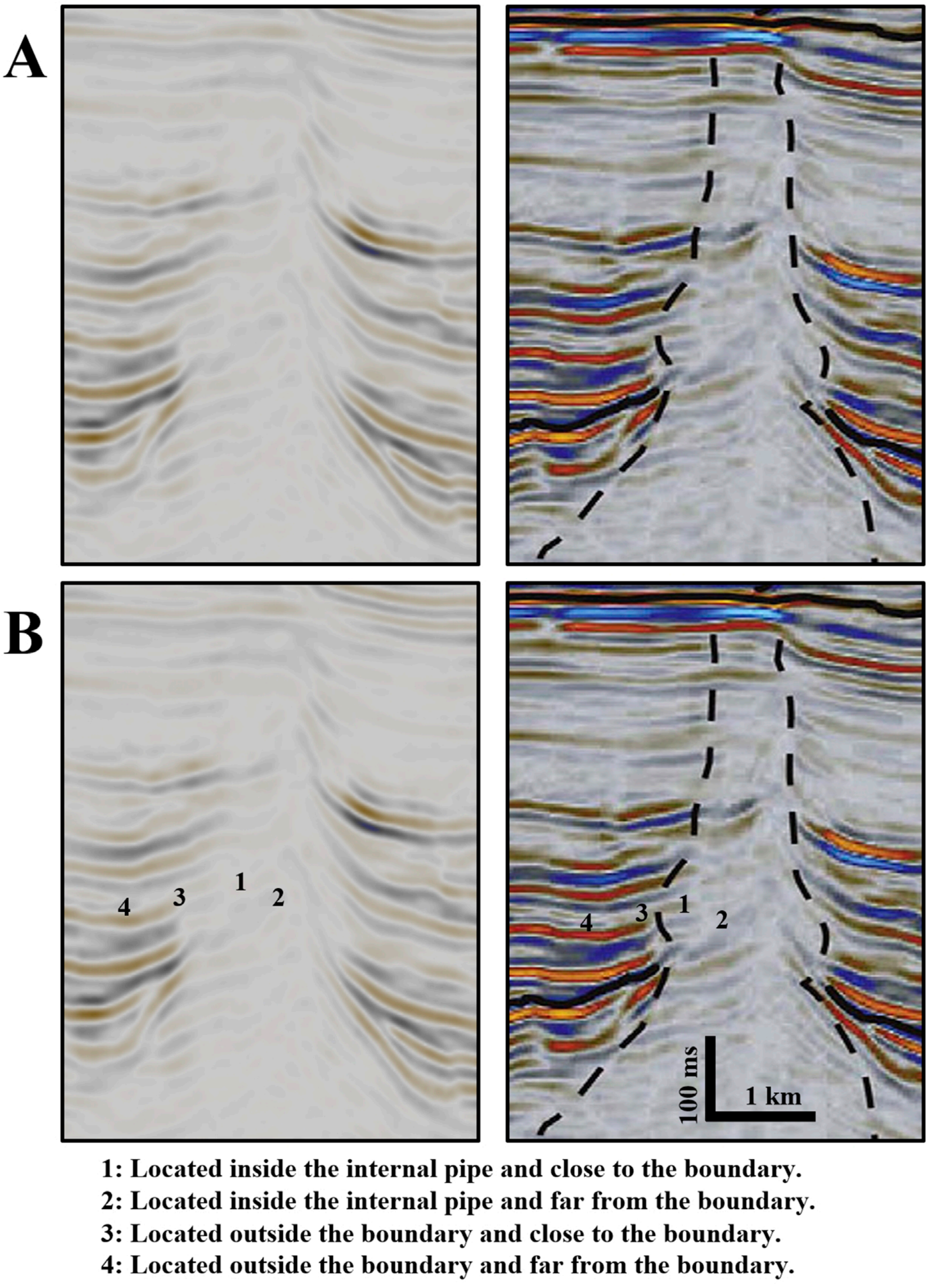

FIGURE 14
Comparison of imaging quality affected by illumination impact, based on real seismic images. The interpretation highlights how variations in illumination influence the clarity and accuracy of seismic imaging in different regions. **(A)** Clean images. **(B)** Interpreted images of P3 in Figure 3. The left side shows the original amplitude, while the right side shows the AGC 'Boosted' images. We observe that points near the boundary edge (1 and 3) present unclear images, likely due to illumination loss rather than resolution loss. In contrast, Points 2 and 4 show relatively stronger amplitude, with Point 4 noticeably stronger than Point 2, likely due to the overall illumination loss in the internal pipe.

understanding of pipe-like geological structures under various illumination scenarios. The 3D illumination analysis reveals significant illumination loss within the internal conduit, attributed to sharp boundary walls and high curvature, leading to resolution deficiencies regardless of wave frequency. The poor illumination coverage in pipe-like structures is primarily caused by high velocity impedance contrasts and steep boundary walls, which obstruct ray paths and lead to significant signal loss, particularly in regions close to the boundary, with larger pipes allowing better illumination through wider azimuths and offsets. Deeper parts, like the lower conduit and root, exhibit weaker illumination, and shadow zones from the top layer further diminish visibility. The study also highlights the crucial role of steep boundary structures, which limit ray penetration due to high velocity contrasts between the pipe and surrounding materials. Furthermore, high hit count multiples caused by external sealing layers around the pipe hinder wave penetration, suggesting that wider azimuth surveys may be needed for better illumination. A comparison with real seismic data from the Loyal field validates the ray-tracing results, showing similar illumination trends near pipe boundaries. Overall, the findings emphasize the importance of considering illumination effects in seismic imaging, particularly for complex subsurface structures, and provide a basis for improving interpretation methods in the exploration of pipe-like formations. These findings emphasize the need for improved seismic acquisition and interpretation methods to better handle similar subsurface pipe-like complexities.

Data availability statement

The original contributions presented in the study are included in the article/supplementary material, further inquiries can be directed to the corresponding author.

Author contributions

ZC: Conceptualization, Methodology, Software, Visualization, Writing–original draft, Writing–review and editing. FT: Methodology, Validation, Visualization, Writing–review and editing. OT: Validation, Writing–review and editing.

Funding

The author(s) declare that financial support was received for the research, authorship, and/or publication of this article. This study received support from the Chinese Scholarship Council and the University of Aberdeen.

Acknowledgments

Special thanks to British Petroleum for permitting the use of their data and granting access to the 4D seismic PSTM dataset of the Loyal Field. Thanks also go to express our gratitude to NORSAR Innovation for providing the academic license for SeisRox Pro.

Conflict of interest

The authors declare that the research was conducted in the absence of any commercial or financial relationships that could be construed as a potential conflict of interest.

Publisher's note

All claims expressed in this article are solely those of the authors and do not necessarily represent those of their affiliated organizations, or those of the publisher, the editors and the reviewers. Any product that may be evaluated in this article, or claim that may be made by its manufacturer, is not guaranteed or endorsed by the publisher.

References

Botter, C., Cardozo, N., Lecomte, I., Rotevatn, A., and Paton, G. (2017). The impact of faults and fluid flow on seismic images of a relay ramp over production time. *Pet. Geosci.* 23, 17–28. doi:10.1144/petgeo2016-027

Cartwright, J., Huuse, M., and Aplin, A. (2007). Seal bypass systems. *Bulletin* 91, 1141–1166. doi:10.1306/04090705181

Cartwright, J., and Santamarina, C. (2015). Seismic characteristics of fluid escape pipes in sedimentary basins: implications for pipe genesis. *Mar. Petroleum Geol.* 65, 126–140. doi:10.1016/j.marpetgeo.2015.03.023

Davide, O., Evans, S., Iacopinic, D., Kabird, M., Masellie, V., and Jackson, C. A.-L. (2021). Leaky salt: pipe trails record the history of cross-evaporite fluid escape in the northern Levant Basin, Eastern Mediterranean. *Basin Res.* 33 (3), 1798–1819. doi:10.1111/bre.12536

Davies, R. J. (2003). Kilometer-scale fluidization structures formed during early burial of a deep-water slope channel on the Niger Delta. *Geology* 31, 949. doi:10.1130/G19835.1

Dean, K., McLachlan, K., and Chambers, A. (1999). "Rifting and the development of the faeroe-shetland basin," in *Geological society, London, petroleum geology conference series* (Geological Society of London), 533–544.

Doré, A. G., Lundin, E. R., Birkeland, Eliassen, P. E., and Jensen, L. N. (1997). The NE Atlantic margin: implications of late mesozoic and cenozoic events for hydrocarbon prospectivity. *Pet. Geosci.* 3, 117–131. doi:10.1144/petgeo.3.2.117

Doré, A. G., Lundin, E. R., Jensen, L. N., Birkeland, O., Eliassen, P. E., and Fichler, C. (1999). Principal tectonic events in the evolution of the northwest European Atlantic margin. *Pet. Geol. Conf. Proc.* 5, 41–61. doi:10.1144/0050041

Gjøystdal, H., Iversen, E., Lecomte, I., Kaschwich, T., Drottning, Å., and Mispel, J. (2007). Improved applicability of ray tracing in seismic acquisition, imaging, and interpretation. *GEOPHYSICS* 72, SM261–SM271. doi:10.1190/1.2736515

Hansen, J. P. V., Cartwright, J. A., Huuse, M., and Clausen, O. R. (2005). 3D seismic expression of fluid migration and mud remobilization on the Gjallar Ridge, offshore mid-Norway. *Basin Res.* 17, 123–139. doi:10.1111/j.1365-2117.2005.00257.x

Huuse, M., and Mickelson, M. (2004). Eocene sandstone intrusions in the Tampen Spur area (Norwegian North Sea Quad 34) imaged by 3D seismic data. *Mar. Petroleum Geol.* 21, 141–155. doi:10.1016/j.marpetgeo.2003.11.018

Jones, I. F., and Davison, I. (2014). Seismic imaging in and around salt bodies. *Interpretation* 2, SL1–SL20. doi:10.1190/INT-2014-0033.1

Judd, A., and Hovland, M. (2007). *Seabed fluid flow impact Geol. Biol. Mar. Environ.* doi:10.1017/CBO9780511535918

Laurain, R., Vinje, V., and Strand, C. (2004). Simulated migration amplitude for improving amplitude estimates in seismic illumination studies. *Lead. Edge* 23, 240–245. doi:10.1190/1.1690896

Løseth, H., Gading, M., and Wensaas, L. (2009). Hydrocarbon leakage interpreted on seismic data. *Mar. Petroleum Geol.* 26, 1304–1319. doi:10.1016/j.marpetgeo.2008.09.008

Løseth, H., Wensaas, L., Arntsen, B., Hanken, N. M., Basire, C., and Graue, K. (2011). 1000 m long gas blow-out pipes. *Mar. Petroleum Geol.* 28, 1047–1060. doi:10.1016/j.marpetgeo.2010.10.001

Maestrelli, D., Iacopini, D., Jihad, A. A., Bond, C. E., and Bonini, M. (2017). Seismic and structural characterization of fluid escape pipes using 3D and partial stack seismic from the Loyal Field (Scotland, UK): a multiphase and repeated intrusive mechanism. *Mar. Petroleum Geol.* 88, 489–510. doi:10.1016/j.marpetgeo.2017.08.016

Mavko, G., Mukerji, T., and Dvorkin, J. (2009). *The rock physics handbook: tools for seismic analysis of porous media*. 2nd Edn. Cambridge: Cambridge University Press. doi:10.1017/CBO9780511626753

Moss, J. L., and Cartwright, J. (2010). 3D seismic expression of km-scale fluid escape pipes from offshore Namibia: 3D seismic expression of km-scale fluid escape pipes. *Basin Res.* 22, 481–501. doi:10.1111/j.1365-2117.2010.00461.x

Nanda, N. C. (2016). *Seismic data interpretation and evaluation for hydrocarbon exploration and production*. Cham: Springer International Publishing. doi:10.1007/978-3-319-26491-2

Petersen, C. J., Bünz, S., Hustoft, S., Mienert, J., and Klaeschen, D. (2010). High-resolution P-Cable 3D seismic imaging of gas chimney structures in gas hydrated sediments of an Arctic sediment drift. *Mar. Petroleum Geol.* 27, 1981–1994. doi:10.1016/j.marpetgeo.2010.06.006

Ritchie, J. D., Johnson, H., Quinn, M. F., and Gatliff, R. W. (2008). The effects of Cenozoic compression within the Faroe-Shetland Basin and adjacent areas. *Geol. Soc. Lond. Spec. Publ.* 306, 121–136. doi:10.1144/SP306.5

Roberts, D. G., Thompson, M., Mitchener, B., Hossack, J., Carmichael, S., and Bjørnseth, H. M. (1999). Palaeozoic to tertiary rift and basin dynamics: mid-Norway to the bay of biscay - a new context for hydrocarbon prospectivity in the deep water frontier. *Pet. Geol. Conf. Proc.* 5, 7–40. doi:10.1144/0050007

Sørensen, A. B. (2003). Cenozoic basin development and stratigraphy of the Faroes area. *Pet. Geosci.* 9, 189–207. doi:10.1144/1354-079302-508

Sun, H., Yue, Y., and Li, M. (2021). 2D Born forward modeling for visco-acoustic media using Gaussian beam. *Chin. J. Geophys.* 64 (2), 637–644. doi:10.6038/cjg2021O0284

Sun, H., Zhang, J., Xue, Y., and Zhao, X. (2024). Seismic inversion based on fusion neural network for the joint estimation of acoustic impedance and porosity. *IEEE Trans. Geosci. Remote Sens.* 62, 1–10. doi:10.1109/TGRS.2024.3426563

Vinje, V., Iversen, E., and Gjøystdal, H. (1993). Traveltime and amplitude estimation using wavefront construction. *GEOPHYSICS* 58, 1157–1166. doi:10.1190/1.1443499

Watson, D., Schofield, N., Jolley, D., Archer, S., Finlay, A. J., Mark, N., et al. (2017). Stratigraphic overview of palaeogene tuffs in the faroe–shetland basin, NE atlantic margin. *J. Geol. Soc.* 174, 627–645. doi:10.1144/jgs2016-132

Yilmaz, Ö. (2018). *Seismic data analysis: processing, inversion, and interpretation of seismic data*. Tulsa: Society of Exploration Geophysicists.

Yue, Y., Sun, H., Wu, R., and Shi, Y. (2021). Gaussian beam born modeling for single-scattering waves in visco-acoustic media. *IEEE Geosci. Remote Sens. Lett.* 18, 1486–1490. doi:10.1109/LGRS.2020.3015906

Zong, J., Chen, Y., Lu, C., Hu, G., and Wo, Y. (2022). Structure-oriented mapping of the subsalt fractured reservoir by reflection layer tomography from a perspective of the zero-offset vertical seismic profiling. *IEEE Trans. Geosci. Remote Sens.* 60, 1–11. doi:10.1109/TGRS.2022.3210046

Zong, J., Stewart, R. R., Yang, J., Dyaur, N., and Wo, Y. (2023). Investigating seismic mode conversions from an ultra-high-velocity caprock by physical modelling, numerical simulations and a Gulf of Mexico salt proximity VSP survey. *Geophys. J. Int.* 234, 1430–1446. doi:10.1093/gji/ggad151